

Experimental determination of pyroxene compositions in the system CaO–MgO–Al₂O₃–SiO₂ at 900–1200°C and 10–15 kbar using PbO and H₂O fluxes

GAUTAM SEN¹

Department of Earth and Space Sciences
University of California, Los Angeles, California 90024

Abstract

Compositions of coexisting orthopyroxenes and clinopyroxenes in the simple systems CaO–MgO–SiO₂(CMS) and CaO–MgO–Al₂O₃–SiO₂(CMAS) were investigated at 9.5–15 kbar pressure and 900–1200°C, using gel, glass and crystalline starting materials. Both Al and Ca contents of coexisting pyroxenes were reversed using Al-, Ca-oversaturated and undersaturated starting mixes. PbO flux was used in all runs, except two, 14.5 kbar, 900°C and 15 kbar, 1000°C, in which H₂O flux was used. Run duration varied between 6 hrs. and 1 week. A melt phase was present in all the charges, and large (~100 μm) crystals were grown. Chemical etching with NH₄HF₂ and polished thin section of the run products revealed the presence of pyroxene crystals of three morphologic types: (1) coarse, euhedral-subhedral (50–100 μm), (2) finer, equant (1–20 μm) and (3) lath-shaped quench crystals (variable size) in glass. Type (2) is generally the predominant type, and exhibits minimum compositional variation in a run. It is also closest to equilibrium composition, as inferred from reversal paired runs.

In reversal paired runs on the system CMAS, variable degrees of overlap in composition of each pyroxene from the “upward” and “downward” runs were observed. The present study indicates that within the spinel peridotite field (1) (Al₂O₃)_{opx} and (Al₂O₃)_{opx} isopleths are strongly dependent on *T* and insensitive to *P*, (2) Well's (1977) thermometer, based on an ideal solution model, should be most useful for estimation of temperature of equilibration of natural spinel peridotites.

Introduction

Thermal and compositional structure of the earth's upper mantle has been a subject of major interest in recent years. Spinel peridotite constitutes a large part of the uppermost upper mantle beneath oceanic areas, as well as in some continental areas (Ringwood, 1975). This rock type occurs commonly as inclusions in alkaline lavas and also as large bodies in ophiolites. Spinel peridotite has also been dredged from the ocean floor (Banatti and Hamlyn, 1980). Various attempts have been made to deduce the temperature (*T*)–pressure(*P*) equilibration of these spinel peridotites in the mantle, using experimentally derived pressure(*P*)–temperature(*T*)–composition(*X*) relations of simple system analogs (for example MacGregor and Basu, 1976; Sen, 1983).

Early synthesis experiments on the system MAS (MgO–Al₂O₃–SiO₂) by MacGregor (1974) indicated that (Al₂O₃)_{opx}^{sp.per.} (i.e., Al₂O₃ content of orthopyroxene in spinel peridotite) is sensitive to both *P* and *T* conditions of equilibration. The results of his study were later found to be inconsistent with geologic observations (Wilshire and Jack-

son, 1975), thermodynamic criteria (e.g., Obata, 1976), and with the results of a subsequent, well-reversed study by Danckwerth and Newton (1978). It now appears, on the basis of the studies on the system MAS by various workers (e.g., Obata, 1976; Fujii, 1976; Danckwerth and Newton, 1978; Lane and Ganguly, 1980), that (Al₂O₃)_{opx}^{sp.per.} is insensitive to *P* conditions of equilibration.

A recent experimental study by Dixon (1980) on the system CMAS (CaO–MAS) suggested that (Al₂O₃)_{opx}^{sp.per.} isopleths may show considerable negative slope (in contrast to the slightly positive isopleths of Danckwerth and Newton), raising the hopes for a possible (Al₂O₃)_{opx}^{sp.per.} geobarometer. Two major problems with relevant studies (e.g., Fujii, 1977; Herzberg and Chapman, 1976) in the CMAS system in the spinel peridotite field are (1) no clear-cut demonstrations of equilibrium with ‘reversal’ type experiments and (2) absence of actual analyses of the pyroxenes. The purpose of the present study was to determine if compositional parameters of pyroxenes in spinel peridotites can be used as *P*, *T* indicators.

A major problem in studying subsolidus equilibria is slow diffusion rates which inhibit equilibration and grain growth. In order to circumvent this problem, H₂O flux was used for the runs at 900°C, 14.5 kbar, and 1000°C, 15 kbar, and PbO flux was used in all other runs. The addition of

¹ Present address: Department of Geology, Florida International University, Tamiami Campus, Miami, Florida 33199.

fluxes caused partial melting, which promoted equilibration and grain growth.

The CMAS system was chosen because it contains the four components which comprise about ninety percent by weight of a natural spinel peridotite. Thus, this system is good approximation of the natural multicomponent system. The present study clearly shows the difficulty in obtaining equilibration in the system, even in long-duration runs in the presence of a melt phase. Several experiments were repeated, and even then the scatter in coexisting pyroxene compositions at any experimental P, T condition could not be completely minimized to unique compositions. Experiments with gel, glass, and crystalline starting materials were carried out in order to qualitatively document the degree of difficulty in obtaining equilibration with various starting materials. Polished sections and doubly-polished thin sections of the run products were made, and a special effort was made to correlate crystal morphology vs. composition of pyroxenes in the experimental runs.

The experimental approach

Demonstration of equilibrium compositions of coexisting pyroxenes in the system CMAS is very difficult inasmuch as both the clinopyroxene and orthopyroxene are solutions of $\text{CaMgSi}_2\text{O}_6\text{-Mg}_2\text{Si}_2\text{O}_6\text{-CaAlAlSiO}_6\text{-MgAlAlSiO}_6$. The present approach can be explained with reference to Figure 1, which schematically shows the pyroxene solvus in $T\text{-}X$ space (P assumed to be constant) as it would be depicted in the plane CaTs-MgTs-Di-En . Note that clinopyroxene dissolves more En and CaTs components with higher temperatures in the spinel peridotite field. Similarly, a temperature increase results in greater dissolution of Di and MgTs components in opx_{ss} . Therefore, compositions of aluminous clinopyroxene solid solution and aluminous orthopyroxene solid solution would fall along some curved lines like $\text{C}_1\text{-C}_2$ and $\text{O}_1\text{-O}_2$ respectively. The equilibrium compositions of coexisting pyroxenes at any given P, T will have to be reversed with respect to two components for each pyroxene: CaTs and En in cpx_{ss} and MgTs and Di in opx_{ss} . Let us suppose that at a temperature T_1 the coexisting clino- and orthopyroxenes in equilibrium with $\text{Fo} + \text{Sp}$ are represented by l_2 and l_1 respectively. The compositions of l_2 and l_1 could be determined in four ways: (a) using $\text{Di} + \text{En} + \text{Sp}$ as a starting mix, which will transform into the assemblage $l_2\text{-}l_1\text{-Fo}$, (b) using a mix that contains $\text{Fo} + \text{Sp}$ and Al-oversaturated clino- and orthopyroxenes which are also undersaturated and oversaturated, respectively, with respect to Ca. In this approach the plane $\text{C}_2\text{-O}_2\text{-Fo} (+\text{Sp})$, for Al-saturation at a temperature higher than T transforms into the plane $l_2\text{-}l_1\text{-Sp} (+\text{leftover Fo})$. The reactions (c) and (d) below are simple tie-line rotations: (c) starting mix $\text{C}_1\text{-O}_2\text{-Sp} (+\text{Fo})$ should give at T_1 , $l_2\text{-}l_1\text{-Sp} (+\text{Fo})$ by simply progressively enriching the cpx_{ss} C_1 in En and CaTs; (d) starting mix $\text{O}_1\text{-C}_2\text{-Sp} (+\text{Fo})$ will do just the reverse. Thus, combination of (a) and (b) or (c) and (d) will essentially reverse

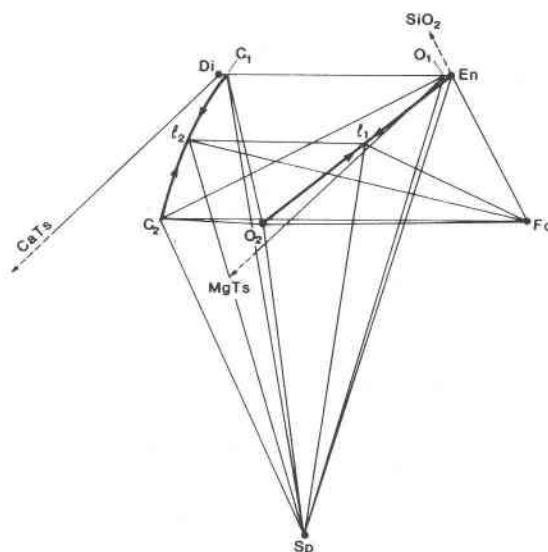


Fig. 1. A schematic $T\text{-}X$ isobaric section through the tetrahedron CMAS (see Fig. 5a) showing possible aluminous pyroxene_{ss} compositions. C_1C_2 and O_1O_2 represent subsolidus cpx_{ss} and opx_{ss} compositions, respectively. The equilibrium coexisting pyroxenes at a given temperature T_1 are represented by l_1 and l_2 , which can be produced by using four different combinations of Al- and Ca-oversaturated and undersaturated starting mixes: (a) $\text{Di-En-Sp} (+\text{Fo})$, (b) $\text{C}_2\text{-O}_2\text{-Fo} (+\text{Sp})$, (c) $\text{C}_1\text{-O}_2\text{-Sp} (+\text{Fo})$, and (d) $\text{O}_1\text{-C}_2\text{-Sp} (+\text{Fo})$. In all experiments of the present study the combinations of (a) and (b) starting mixes were used. Only two runs with (c) and (d) were performed to confirm the results obtained from (a) and (b). See text for further discussion.

the position of l_1 and l_2 ($+\text{Sp}$ for Al-saturation). Products of each of these four starting mixes should show these reactions: in (a) both cpx_{ss} and opx_{ss} should show dissolution reaction; (b) both cpx_{ss} and opx_{ss} should show exsolution reactions (c) cpx_{ss} and opx_{ss} should show dissolution and exsolution reactions, respectively, and (d) cpx_{ss} and opx_{ss} should show exsolution and dissolution reactions, respectively.

In actual experiments, reaction kinetics, grain size and grain intergrowth cause serious problems. Also, none of the "exsolution" data described here are truly exsolution inasmuch as there is also dissolution and reprecipitation of pyroxenes (quench) from the melt phase (since a flux was used to cause melting). Experimental difficulties are discussed later. In the present study, (a) and (b) coupled runs were carried out at 9–15 kbar and 900–1200°C; and two (c) and (d) coupled runs were carried out at 12.5 kbar, 950 and 1050°C. Data on the run products of (c) and (d) mixes are given in Appendix IV. All the results appear to be internally consistent.

Experimental methods

Crystals of orthoenstatite and diopside were prepared from gel at 1 atm. and 800°C for 48 hours with several intermediate crushings. All the gels (15 g each) were prepared from Mg-metal, Al-

Table 1. Composition of the starting materials used in synthesis and reversal runs

Mix/Crystals	SiO ₂	CaO	Al ₂ O ₃	MgO	Remarks
Aluminous opx	53.71	1.52	9.09	34.57	
Aluminous cpx	51.20	20.56	9.20	18.83	Prepared from gel (see text)
Enstatite	59.85	-	-	40.15	
Diopside	55.49	25.90	-	18.61	
Mixes for CMS system					
CMS 1	En ₃₃	Di ₆₇			Mechanical mix of en, di crystals
CMS 1a	En ₃₀	Di ₆₄	Q ₆		Mechanical mix of crystals of en, di, q.
Mixes for CMAS system					
CMAS	(SiO ₂) _{42,46} (CaO) _{11,90} (Al ₂ O ₃) _{19,60} (MgO) _{2,64}				Gel
CMAS 1X	En _{25,7} Di _{43,3} SP _{28,0} Q ₃				Mechanical mix of crystalline materials
CMAS-1Y	(SiO ₂) ₄₅ (CaO) ₁₁ (Al ₂ O ₃) ₁₈ (MgO) ₂₆				Glass
CMAS-2X	(En ₃₃ Di ₆₇) _{66,7} SP _{26,7} Q _{6,6}				Mechanical mix of crystalline materials
CMAS-2Y	(Al-en) _{33,3} (Al-di) _{33,3} SP _{26,7} Q _{6,7}				"
CMAS-H-2	(En ₃₃ Di ₆₇) ₇₅ SP ₂₀ Q ₅				"
CMAS-H-1	(Al-en) ₅₀ (Al-di) ₅₀ 75SP ₂₀ Q ₅				"

Note: All values are in wt. percent

metal, CaCO₃ and tetraethylorthosilicate (for SiO₂) following the method outlined by Hamilton and Henderson (1968). Spinel was partially crystallized from gel at 1800°C for 30 min. in a radio-frequency induction furnace; some dehydrated gel remained. Aluminous orthopyroxene and aluminous clinopyroxene (compositions given in Table 1) crystals were separately prepared from gels of respective compositions at 1250°C, 15 kbar in the presence of H₂O in welded Pt-capsules in a piston-cylinder apparatus. One intermediate crushing and 48 hours of total run duration yielded aluminous pyroxenes with fairly well developed X-ray powder diffraction patterns.

10 g of the glass starting material CMAS-1Y (Table 1) was made in a radio-frequency induction furnace, with intermediate grinding and remixing. All runs were made in a 2.54-cm-diameter piston-cylinder apparatus with talc as the pressure medium. The experimental set-up is similar to that described by Boettcher (Johannes et al., 1971). Each reversal run was made with two graphite capsules, sealed inside a Pt-capsule: one graphite capsule contained a nearly equimolar proportion of enstatite, diopside, and spinel along with 6 to 23 wt.% PbO (or a trace to 1 wt.% H₂O) and 1 to 7 wt.% quartz. The other graphite capsule contained spinel, the aluminous cpx and aluminous opx shown in Table 1, and similar amounts of PbO (or H₂O) and quartz. Graphite was used as capsule material because PbO was found to react with Pt. Many synthesis runs with gels were also made (Table 2). The reconnaissance-type runs with PbO indicated that the PbO-rich melt dissolves SiO₂ at significantly higher amounts than the other components at any given *P,T* (Table 3). This caused total disappearance of orthopyroxene from the run products at times. A slight excess of SiO₂ was added to partially compensate for this effect such that both orthopyroxene and forsterite occurred. However, in a few of the coupled reversal runs, quartz, instead of forsterite, was present in the run products. Separate synthesis runs with forsterite at similar conditions yielded pyroxenes with compositions overlapping the corresponding runs with quartz. Thus,

presence or absence of quartz does not seem to have any profound effect on the pyroxene compositions, as long as spinel is present (cf. Howells and O'Hara, 1975; Lindsley and Dixon, 1976).

Temperature was measured with Pt₁₀₀-Pt₉₀Rh₁₀₀ thermocouples. A Eurotherm controller was used to control the temperature within 4°C. All runs were of hot piston-out type, i.e., they were overpressurized by 1.5 to 3 kbar, brought up to desired temperature, and then the excess pressure was reduced. For the first few hours of each experiment, the pressure continuously increased by thermal expansion of the assembly, and had to be reduced. Pressure-calibration was done against the reaction albite = jadeite + quartz as suggested by Johannes et al. (1971). The pressures quoted in Table 2 are nominal values (±0.25kbar) without any friction-correction added to them.

The run products were examined and analyzed with a microscope and an automated microprobe (ARL model EMX). Analytical conditions include 15 kV accelerating potential, 30 nA beam current, 1 μm beam diameter. Standards used were Mg₃Al₂Si₃O₁₂ glass, and a wollastonite. Initial qualitative determination was done with Energy Dispersive Spectrometry. All quantitative wavelength-dispersive spectrometric analyses were carried out using a Tracor-Northern (NS-880) automation system. Reproducibility was periodically checked by analyzing these standards and a synthetic diopside.

Much of the subtle microstructures in the run products became clear upon etching with dil. NH₄HF₂. In the present study, the finer grained charges were etched with dil. NH₄HF₂ (2% solution) for 10 min. at 22°C. After etching they were washed with distilled H₂O, dipped in Na₂CO₃ solution for 5 min., and rinsed with H₂O, citric acid, and ethyl alcohol, following the method of Wegner et al. (1978). Microprobe analysis was carried out several times on each charge: first on a polished section of the charge, then on the etched sample, followed by another set of analyses on the doubly polished thin section. Repeated analyses ensured that etching had no effect on compositions of the pyroxenes, but it dissolved some of the PbO-rich silicate glass. Also, energy dispersive spectra of the various mineral phases did not show the presence of Pb in any of them. It must, however, be mentioned that no wave-length dispersive analysis was done with respect to Pb.

Experiments in the CaO-MgO-SiO₂

Three "dissolution"-type runs (e.g., Warner and Luth, 1974; Lindsley and Dixon, 1976) in the CMS system were made to characterize crystal morphology-composition relations, so that such relations could be utilized to identify equilibrium composition of coexisting ortho- and clinopyroxenes in the more complex CMAS system. The subsolidus pyroxene phase relations of the CMS system have been well documented by previous workers (e.g., Lindsley and Dixon, 1976), and also, this system is compositionally close to the system of the present study. Therefore, the study of the CMS system using PbO flux was carried out before using the same technique for experimenting on the CMAS system.

The three CMS runs were carried out at 10 kbar, 1000°C, 15 kbar, 1200°C, and at 15 kbar, 1000°C (Table 2). In each of these three runs three morphologic types of pyroxene occur: (1) euhedral, phenocrystic (Fig. 2a), (2) small, abundant, groundmass-type (Fig. 2a) and (3) feathery, elongated, partly radial, quench crystals embedded in glass (Fig. 2b). Types (1) and (2) show fairly uniform

Table 2. Experimental conditions

Run No.	P(kb)	T(°C)	Duration(h)	PbO(wt%)	H ₂ O(wt%)	Remarks
CMS 1a-1	15	1000	21	10	-	All three morphologic types (see text) present; grains upto 40 μm.
CMS 1a-2	15	1200	24	10	-	Grains upto 100 μm.
CMS 1a-3	10	1000	25	10	-	Grains upto 40 μm.
CMAS-1	10	1000	25	12	-	Spinel occurring in clusters; melt inhomogeneously distributed.
CMAS-5	9.5	1000	12	12	-	Anorthite (containing 2 wt% PbO) present.
CMAS-2X) CMAS-2Y) 2a	10	900	24	25	-	Both capsule have melt, euhedral spinel, and pyroxenes of three morphologic types. The CMAS-2Y part was crushed and rerun (below). (%melt = 10). CMAS-2X and a small piece of CMAS-2Y were analyzed.
CMAS-2X) CMAS-2Y) 2	10	900	52	25	-	One capsule contained the product of CMAS-2Y above, and the other had new CMAS-2x starting material. (%melt = 12)
CMAS-2X) CMAS-2Y) 3a	12.5	900	22	25	-	Product of CMAS-2Y starting material was ground and rerun (below).
CMAS-2X) CMAS-2Y) 3b	12.5	900	43	25	-	One capsule contained the product above and the other contained new CMAS-2X starting material. Both contain grains upto 50 μm. 15% melt present in each.
CMAS-1X) CMAS-1Y) 3a	14.5	1200	24	6	-	The double capsule was not taken out, but the T was dropped to 900°C (below).
CMAS-1X) CMAS-1Y) 3	14.5	900	96	6	-	The glass starting material (CMAS-1Y) gave very fine crystal intergrowths -- no decent probe analysis obtained. CMAS-1X gave 60 μm crystals.
CMAS-H1) CMAS-H2) 4	14.5	900	45	-	1	Fairly large crystals (50 μm) in both capsules. Garnet was sought for but could not be found.
CMAS-1X) CMAS-1Y) 2	15	1000	47	8	-	CMAS-1Y (glass starting material) again gave too fine crystals -- could not probe.
CMAS-H1) CMAS-H2) 5	15	1000	35	-	tr.	Crystalline starting materials in both capsules gave 60 μm grains. Melt present.
CMAS-H1) CMAS-H2) 2	12.5	1000	6	-	tr.	Fairly large grains were obtained with CMAS-H2 starting material. Too much melt and absence of cpx in capsule with CMAS-H1 starting material.
CMAS-1X) CMAS-2Y) 1	15	1200	24	8	-	Fairly large euhedral crystals of enstatite and smaller equant diopside crystals present. Euhedral spinel crystals are generally confined to glass-rich areas in both capsules.
CMAS-1X) CMAS-2Y) 2'	12.5	1150	48	8	-	Similar to above.
CMAS-1X-R1	15	1100	6	8	-	The run was held at this T,P for 6 hrs, and then the T,P were dropped to the conditions below without taking the capsule out.
"	12.5	1000	168	8	-	Fairly large coarse-grained run product. Overall grain size and morphologic variations similar to other runs. The longer duration did not help grain growth or equilibration significantly.
CMAS-1X-R2	13	900	24	8	-	The run was held at this P,T for 24 hrs, and then was rerun below after grinding.
"	10	1000	168	8	-	Run products similar in texture to other coarse grained run products.

extinction, but type (3) always exhibits radial (nonuniform) extinction. While orthopyroxene formed all three types, clinopyroxene rarely crystallized as type (3). Glass inclusions are abundant in types (2) and (3) and less so in type (1).

Doubly-polished thin sections of the charges showed common presence of twinning in type (1) pyroxenes. In terms of relative abundance, type (2) is the most abundant type; abundance of the other two types is directly proportional to the abundance of glass. Glass occurs mostly in

Table 3. Composition of some PbO-rich silicate glasses in the runs

Run #	P(kb)	T(°C)	SiO ₂	CaO	Al ₂ O ₃	MgO	PbO ^d
CMS-3	9	1000	28.87	12.73	17.07	12.07	29.26
CMS-1X-3	14.5	900	41.31	10.10	15.32	13.43	19.85
CMS-1X-R2	10	1000	36.37	9.46	14.00	19.98	20.19
CMS-1X-R1	12.5	1000	30.89	13.42	20.25	10.15	25.30
CMS1a-2	15	1200	48.63	14.53	-	18.03	19.81

d = estimated PbO = (100.00 - oxide sum) wt%

scattered pools, studded with quench crystals. Any microprobe analysis, which did not show an oxide sum = 100 ± 1 and a good structural formula (i.e., for 6 oxygens: $\text{Si} = 2.000 \pm 0.005$, and $\text{Ca} + \text{Mg} = 2.00 \pm 0.004$), was discarded. A Pb-peak was not detected in any of the mineral EDS spectra. Also, the WDS analyses of the minerals showed good totals (100.0 ± 1); therefore, it appears that Pb did not enter in significant amounts into the mineral phases.

Compositionally, a spread in $\text{Ca}/(\text{Ca} + \text{Mg})$ ratios of both clinopyroxenes and orthopyroxenes was observed in a single run. The spread is very tight for the 15 kbar, 1200°C

run, but it is rather broad for the other two runs (Fig. 3). Modal compositions of the pyroxene phases in each run are controlled by the most abundant grains with type (2) morphology. In each of the 15 kbar runs, the most abundant composition also seems to correspond very well with the inferred equilibrium composition of Lindsley and Dixon (1976). The coarse type (1) grains often have a virtually unreacted core and a quench overgrown rim. Commonly, the inferred equilibrium composition was shown not by the rim but by a zone intermediate between rim and core of a type (1) grain. Type (3) grains always gave variable compositions.

The two-pyroxene miscibility gap in the system CMS at 15 kbar is well defined with the experiments of Lindsley and Dixon (1976). Such well-reversed data do not exist for 10 kbar CMS pyroxenes. Lindsley and Dixon presented microprobe analyses of coexisting pyroxenes in an "exsolution"-type run at 10 kbar/1100°C. Mori and Green (1975) presented reversed data at 10 kbar, 900°C and microprobe analytical data on an "exsolution"-type run at 10 kbar, 1200°C. Combining the "exsolution" runs of these workers and "dissolution" runs of Warner and Luth (1974) and the present study, the 10 kbar two-pyroxene miscibility gap up to 1300°C has been constructed (Fig. 3). The in-



(a)



(b)

Fig. 2. Photomicrograph of polished thin sections. (a) run product of CMS 1a-2 (between crossed nicols). Note the twinned euhedral cpx phenocryst ($\sim 100 \mu\text{m}$) in the middle. Subhedral, type (2) grains (see text) are in abundance. The dark areas are mostly glass and some graphite patches. The dark area at the top is the wall of the graphite capsule. Long dimension = 0.4 mm. (b) run product showing quench crystals of opx in glass (between crossed nicols). Long dimension = 0.73 mm.

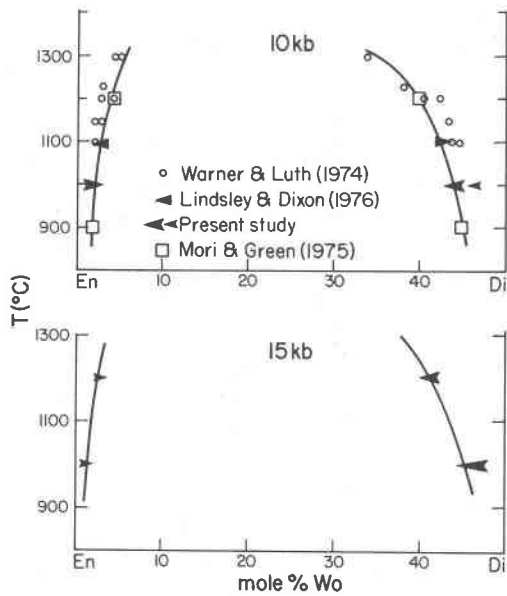


Fig. 3. En-Di miscibility gap at 10 and 15 kbar. The diopside and enstatite limbs at 15 kbar are from Lindsley and Dixon (1976). Length of the arrows in the 15 kbar diagram indicates compositional spread of each pyroxene phase at a given T . The 10 kbar diopside and enstatite limbs are drawn on the basis of data provided by previous studies and this study (see text for details). The small arrow of the present study represents 3 analyses and the big arrow represents 8 analyses on the diopside limb.

ferred 10 kbar miscibility gap compares very well with the Lindsley-Dixon 15 kbar miscibility gap up to 1200°C; above this temperature the miscibility gap is only partly constrained by the Warner-Luth data at 10 kbar. As observed by many previous workers, there is very little pressure effect on the miscibility gap in the CMS system. The P -effect was quantified by Lindsley et al. (1981). They have also estimated the 10 kbar miscibility gap on the basis of a compilation of all available reversed data and a very successful solution model. The 10 kbar miscibility gap of Figure 3 matches well with that of Lindsley et al. up to 1200°C.

CMAS experiments

A series of experiments of equal duration with various starting materials was carried out initially, in order to make a careful selection of starting materials which will grow large crystals and equilibrate rapidly. Glass, gel (with/without seed crystals), and crystalline materials crystallized from gel were all used. At 10 kbar, 1000°C, and for a duration of 25 hours, glass gave the poorest results: the grains were too fine and intergrown, so that a very wide spread in composition of pyroxenes with mostly inferior structural formulae was obtained. Better results were obtained with crystalline starting materials, and particularly if they were ground intermittently and run again at a given P, T condition. All the reversal runs were made with crys-

talline starting materials as double capsule runs outlined in the section on experimental methods.

Noticeable petrographic similarity between the CMS and CMAS run products exists. In the CMAS run products also, three morphologic types were found; euhedral, large crystals (phenocrystic, Figs. 4a and b); small, equant grains (groundmass); and skeletal crystals floating in the glass pool areas. Composition-texture relations are also similar to those observed in the CMS runs, but with a few differences: (1) the larger orthopyroxene grains are relatively more abundant; (2) early spinel, clinopyroxene (and olivine), and especially glass, occur very commonly and completely enclosed inside large orthopyroxene grains (Fig. 4); and (3) zoning and interference are much more complicated in the CMAS pyroxenes. It appears that the large orthopyroxenes (type (1)) initially grew as "hopper" crystals (e.g., Lofgren, 1980), and then the growth was more continuous. Occasionally these large grains have a 3 μm quench rim. Complex zoning features are exhibited by these large grains. The smaller, equant grains, on the other hand, gave a lesser spread in composition. The skeletal crystals (quench) were also analyzed but were not considered while inferring the "equilibrium" composition from a paired run. These crystals gave extremely variable compositions (part of which may represent analytical interference from spinel or olivine, or adjacent/overlapping pyroxene grains).

Ideally, at equilibrium, one should expect the compositions of each of the clinopyroxenes or orthopyroxenes in a paired run (exsolution and dissolution couples) to converge to one point. However, because of the extremely slow diffusion rates involved, a continuous compositional spread for both pyroxenes in each of the paired runs was observed in the present experimental study (Appendices II and III; Fig. 5b). In general, in any given paired run, the Al_2O_3 content of clinopyroxene grains showed a much tighter grouping than the orthopyroxenes. On the other hand, orthopyroxenes showed a very tight grouping in $\text{Ca}/(\text{Ca} + \text{Mg})$ ratio.

Variable degrees of overlap in composition of pyroxenes were observed between individuals of a paired run, a phenomenon which is known as "path looping" (Lane and Ganguly, 1980; Perkins and Newton, 1980). These overlaps were large in some cases—e.g., 15 kbar, 1000°C-orthopyroxenes (Fig. 5b), and very tight in the best case—e.g., 10 kbar, 900°C paired run: both pyroxenes show compositional spread with a tendency to converge. The 10 kbar, 900°C and 12.5 kbar, 900°C paired runs were ground under acetone once after 24 h of run duration, then dried and run again. In some cases of a partial overlap, individual orthopyroxenes (and clinopyroxenes) in a paired run sometimes gave a narrow compositional range (within analytical uncertainty). However, in cases in which this region is slightly larger than permissible analytical uncertainties (e.g., 12.5 kbar, 900°C run), the equilibrium composition is chosen to be the one that lies in this overlap region and represents the mode, assuming that the reaction kinetics were such that the mode represents equilibrium composition. The in-

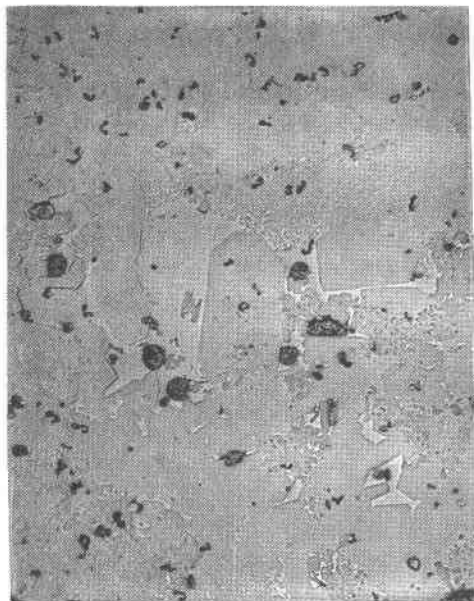


Fig. 4. (a) Photomicrograph (reflected light) of polished section of the run products of CMAS-2X-3. Note the presence of both type (1) and (2) grains. The large euhedral grains near the center field of view are opx. These type (1) opx grains have abundant cpx, glass, and spinel inclusions in their cores, but the outer rims ($\sim 1\text{--}3\ \mu\text{m}$) are generally inclusion-free. (The black patchy materials are graphite. There is a large pool of glass in the middle. (Long dimension = 0.73 mm.) (b) Photomicrograph of a thin section of the run products of CMAS-1X-R1. Note the euhedral, twinned type (1) diopside crystal in the center of field of view. Type (2) crystals are abundant. (Crossed nicols. Long dimension = 0.73 mm).

ferred equilibrium compositions obtained from these reversed experiments are given in Table 4.

It should be pointed out that, even with a dissolution run and a paired run, the equilibrium composition of or-

thopyroxene at 15 kbar, 1000°C could not be well defined (Fig. 5b). Thus, the inferred equilibrium pyroxene compositions at 15 kbar, 1000°C (Table 4) were not used in deriving thermodynamic parameters (discussed below), even though these compositions are thermodynamically consistent with the other runs. The inference regarding equilibrium compositions at this P, T is based on good analyses and modal morphologic (i.e., compositions of most small, equant grains) criteria.

Discussion and conclusions

The overall features of the polybaric two-pyroxene miscibility gap are best seen in Figure 6, in which the CMAS data at 10, 12.5 and 15 kbar are projected from Al_2O_3 onto the join $\text{CaMgSi}_2\text{O}_6\text{--MgSiO}_3$, and compared with the CMS miscibility gap at 10 and 15 kbar. Figure 6 demonstrates that the presence of Al_2O_3 diminishes the apparent solubility of MgSiO_3 in cpx_{ss} . Although natural spinel lherzolite spinels are not close to being pure MgAl_2O_4 , it is clear that any temperature estimated from the $\text{Ca}/(\text{Ca} + \text{Mg})$ ratio of cpx_{ss} , may be much lower than the actual temperature of equilibration of natural spinel lherzolites. Interestingly, Al_2O_3 does not seem to affect the enstatite-limb at all. Part of these differential effects of Al_2O_3 on the two limbs of the miscibility gap must be attributed to the projection scheme adopted here, i.e., projection from Al_2O_3 . Because (1) the cpx_{ss} -limb shows stronger curvature at higher temperatures than the opx_{ss} -limb, and (2) the Al_2O_3 (corner from which the

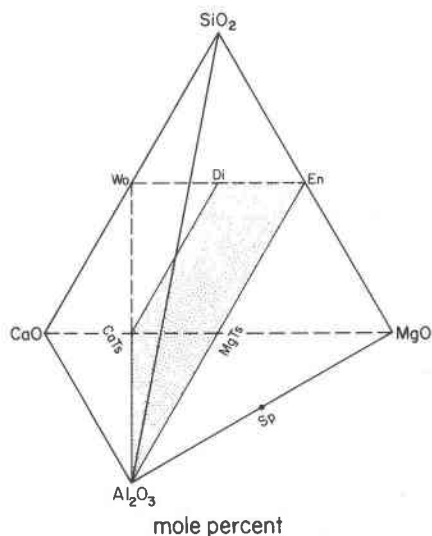


Fig. 5a. The compositional tetrahedron $\text{CaO-MgO-Al}_2\text{O}_3\text{-SiO}_2$; and the aluminous pyroxenes of the present study are represented along the stippled plane diopside ($\text{Di-CaMgSi}_2\text{O}_6$)-enstatite (En-MgSiO_3)-Ca-Tschermak's component ($\text{CaTs-CaAl}_2\text{SiO}_6$)-Mg-Tschermak's component ($\text{MgTs-MgAl}_2\text{SiO}_6$) in (b).

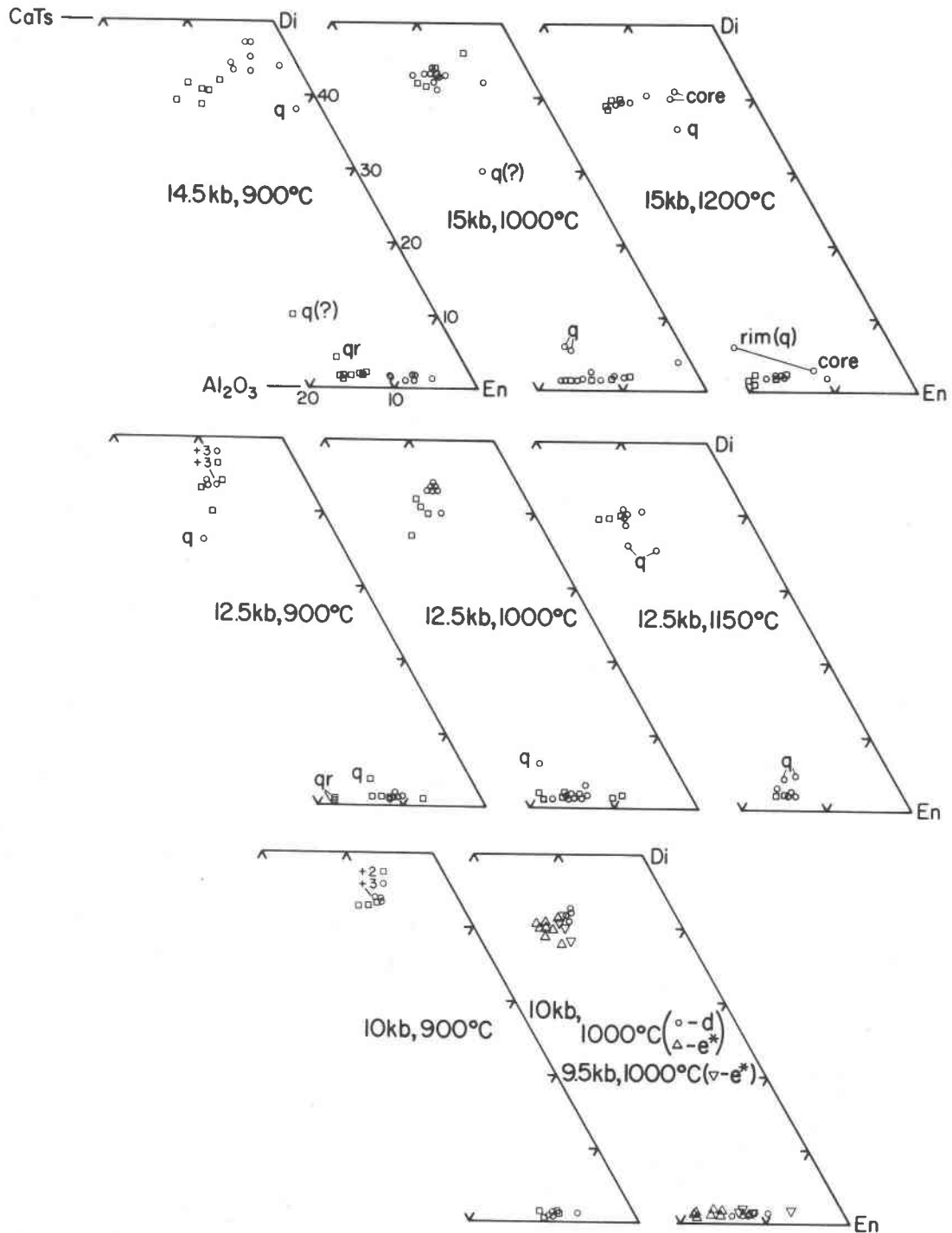


Fig. 5b. Representative pyroxene compositions of the CMAS runs of present study. Squares—exsolution, circles—dissolution. e^* —crystallization from a gel starting material, interpreted to be mostly exsolution-type, q—quench crystals, qr—quench rim on a type (1) crystal. q(?)—no definite quench crystal morphology was apparent.

CMAS pyroxenes are projected) has a relatively more “orthogonal relation” with the opx_{ss} -limb than with the cpx_{ss} -limb due to very low Ca-content of opx_{ss} , the projection-effect should be larger on the cpx_{ss} -limb. The

above statement can be illustrated with Figure 7, in which the coexisting CMAS pyroxenes at 15 kbar, 1200°C and 15 kbar, 900°C are shown as AB and CD, respectively, in the plane $\text{Al}_2\text{O}_3\text{-CaSiO}_3\text{-MgSiO}_3$. Also shown are Al-free

Table 4. Inferred equilibrium compositions of pyroxenes

	12.5 kb, 900°C	14.5 kb, 900°C	10 kb, 900°C	10 kb, 1000°C	12.5 kb, 1000°C	12.5 kb, 1150°C	15 kb, 1200°C	15 kb, 1000°C
SiO ₂	52.33	56.12	52.76	56.85	53.59	56.77	51.86	55.10
CaO	24.46	0.72	23.25	0.93	24.23	0.64	23.40	1.16
MgO	17.65	36.72	18.81	37.82	18.41	37.60	18.02	36.22
Al ₂ O ₃	5.85	4.92	4.87	5.06	4.48	4.94	6.76	6.33

Cations/6 oxygens

Si	1.874	1.908	1.895	1.895	1.908	1.903	1.857	1.872	1.874	1.866	1.840	1.847	1.822	1.823	1.870	1.882
Ca	0.939	0.026	0.895	0.033	0.924	0.023	0.898	0.042	0.913	0.038	0.852	0.058	0.855	0.061	0.906	0.036
Mg	0.942	1.861	1.007	1.879	0.977	1.878	0.959	1.834	0.970	1.827	0.985	1.789	0.961	1.759	0.968	1.829
Al ^{IV}	0.126	0.070	0.105	0.105	0.092	0.097	0.143	0.128	0.126	0.133	0.160	0.153	0.178	0.177	0.130	0.118
Al ^{VI}	0.121	0.075	0.101	0.094	0.096	0.098	0.142	0.126	0.120	0.133	0.163	0.154	0.182	0.179	0.128	0.129
Sum	4.002	3.998	4.002	4.006	3.998	3.999	4.000	4.001	4.003	3.999	3.999	4.000	3.998	4.000	4.001	3.994

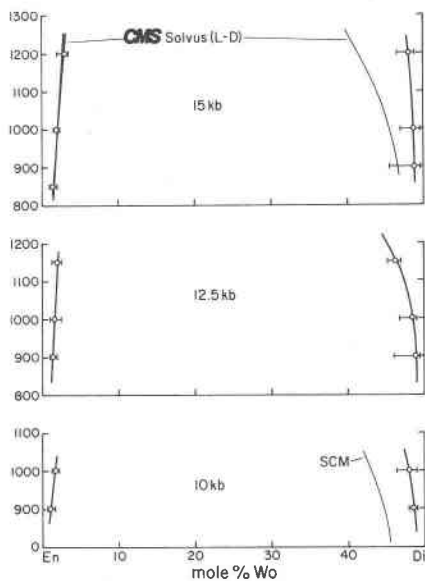


Fig. 6. 10, 12.5, and 15 kbar two-pyroxene miscibility gap in the system CMAS of present study (dark lines) is compared with that in the system CMS at 15 kbar (Lindsley and Dixon (L-D), 1976) and at 10 kbar (as inferred in this study). The brackets represent compositional spread, and the dots represent modal values. Note that all aluminous pyroxene compositions are projected from Al₂O₃ onto the join Di-En. This figure clearly shows that temperatures of mantle lherzolites estimated from Ca/(Ca + Mg) ratio of cpx (which is, in effect, a projection from Al₂O₃, Cr₂O₃, TiO₂, Na₂O, MnO, ...) using the CMS miscibility gap of Lindsley and Dixon (1976), will result in a substantially lower temperature than the actual temperature of equilibration of those rocks. This difference is believed to be purely an artifact of the projection scheme (i.e., from Al₂O₃). (See Fig. 7 and text for further discussion.)

CMS pyroxenes at 15 kbar, 900°C (X₁Y₁) and at 15 kbar, 1200°C (X₂Y₂). Points A', C', B', D' represent the CMAS pyroxene compositions A, C, B, and D, respectively, as projected from Al₂O₃ onto the join CaSiO₃-MgSiO₃. Such a projection is equivalent to recasting the CMAS pyroxene compositions in terms of Ca and Mg. It is clear from this figure that such projection from Al₂O₃ will have a stronger projection effect on the CMAS cpx_{ss}-limb than on the opx_{ss}-limb. The projection-effect is further illustrated by projecting the 15 kbar, 1200°C CMAS cpx_{ss} composition (i.e., point A) from a composition [(CaSiO₃)₃₃(Al₂O₃)₆₇] onto the join CaSiO₃-MgSiO₃: this projected point is p'. Note that p' lies almost on X₂, which is the CMS 15 kbar, 1200°C cpx_{ss}.

Figure 8 shows possible (Al₃O₃)_{opx} and (Al₂O₃)_{cpx} isopleths derived from the inferred equilibrium compositions. The 900 and 1000°C isopleths are fairly well defined, even though the uncertainties are large. It is clear that Al₂O₃-content of these pyroxenes in a four-component spinel peridotite should be very sensitive to temperature, and not pressure, condition of its formation. Figure 8 also brings out the general parallelism between the (Al₂O₃)_{opx} isopleths of the CMAS and MAS systems. However, temperature of equilibration of a natural spinel peridotite estimated from the MAS system (Al₂O₃)_{opx} isopleths should be ~75°C higher than that estimated using similar isopleths in the system CMAS.

A point of interest is Presnall's (1976) experiment at 11 kbar on the CMAS spinel peridotite solidus which gave an apparently equilibrium opx_{ss} with 8% Al₂O₃. This analysis has been repeated more recently by J. Hoover (1984, pers. comm.) and appears to be correct. On the basis of the composition of this opx_{ss}, Presnall (1976) suggested that the (Al₂O₃)_{opx}^{sp-per.}-isopleths in the CMAS system must have

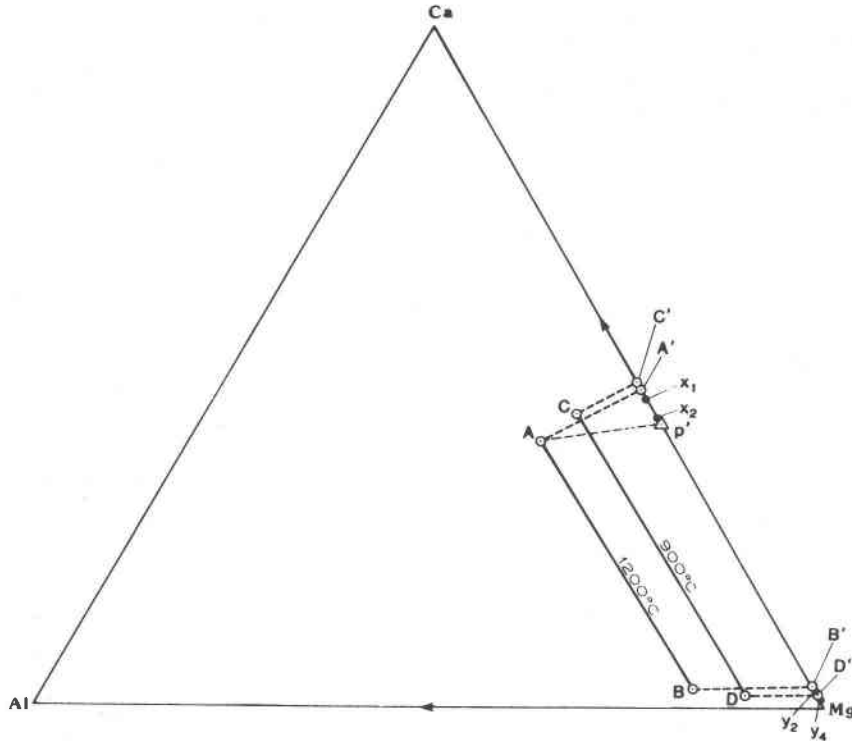


Fig. 7. Mole percent diagram $\text{Al}_2\text{O}_3(\text{Al})\text{-CaSiO}_3(\text{Ca})\text{-MgSiO}_3(\text{Mg})$ showing effect of projection of the CMAS pyroxenes from Al_2O_3 onto the join $\text{CaSiO}_3\text{-MgSiO}_3$. The tie-lines AB and CD represent 15 kbar, 1200°C and 15 kbar, 900°C coexisting CMAS pyroxenes, respectively. C', A', B', D' represent compositions C, A, B, D as projected from Al_2O_3 onto the join $\text{CaSiO}_3\text{-MgSiO}_3$. X_1Y_1 and X_2Y_2 represent 900°C and 1200°C, 15 kbar coexisting CMS pyroxenes. P' is the projected composition of A from an arbitrary projection point $(\text{CaSiO}_3)_{33}(\text{Al}_2\text{O}_3)_{67}$. Details are discussed in the text.

negative dT/dP slopes. Although the CMAS pyroxene phase relations at the solidus have not been clearly worked out, it is possible, based on our knowledge about the CMS system (e.g., Huebner, 1980; Lindsley et al., 1981), that near

the CMAS solidus three aluminous pyroxene phases are present: orthopyroxene_{ss}, pigeonite_{ss}, and cpx_{ss}. Also, it seems possible that various inversion reactions on the CMAS opx_{ss}-limb occur at near-solidus temperatures.

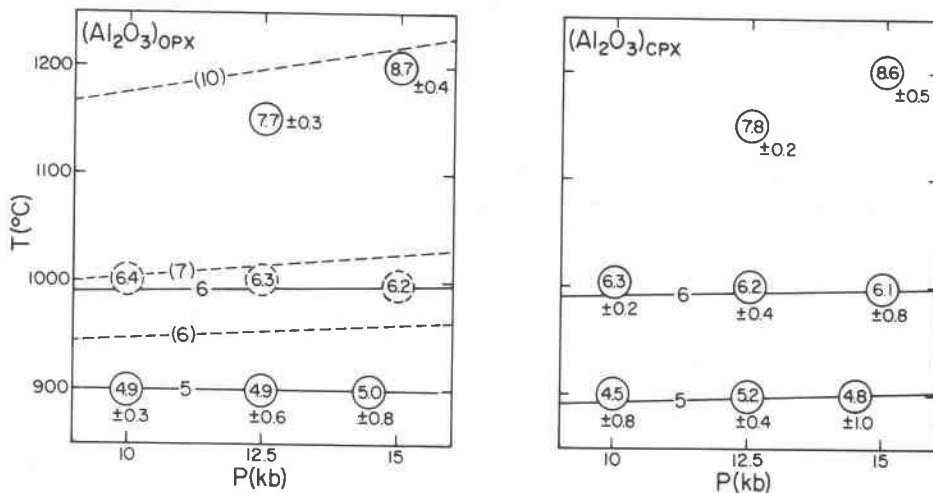
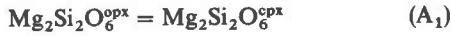


Fig. 8. Wt.% $(\text{Al}_2\text{O}_3)_{\text{opx}}$ and $(\text{Al}_2\text{O}_3)_{\text{cpx}}$ -isopleths in the CMAS system of present study. Continuous lines—my data on CMAS; dashed lines— $(\text{Al}_2\text{O}_3)_{\text{opx}}$ -isopleths in the system MAS, as inferred by Lane and Ganguly (1980). The 1000°C $(\text{Al}_2\text{O}_3)_{\text{opx}}$ numbers in my study of the CMAS system do not provide any tighter constraints to warrant precise "equilibrium" values (see text for discussion), and hence they are shown in dashed circles.

Thus, because of the inherent differences in phase relations between solidus and subsolidus pyroxenes, compositional differences between solidus and subsolidus opx_{ss} should probably be expected. Therefore, Presnall's inferred 8% (Al₂O₃)_{opx}-isopleth is not likely to be correct.

The following reactions determine pyroxene compositions in the presence of Fo in the CMAS system:



Lindsley et al. (1981) and Grover (1980) have extensively discussed the thermodynamic implications of various published solution models for reactions (A₁) and (A₂), and presented a new model that employs an asymmetric Margules formulation for the cpx_{ss} and symmetric Margules formulations for the opx_{ss}.

Since Lindsley et al.'s (1981) model correctly reproduces the phase relations (especially the pigeonite stability field) and all existing well reversed experimental data on pyroxenes in the system CMS, it is useful to compare the presently obtained data with their model. Their temperature equations for reactions (A₁) and (A₂) (given as A and B respectively in Lindsley et al., 1981) are used to compare the presently obtained CMAS data with the CMS data (Table 5). Table 5 also shows a comparison of temperature estimates based on Wells's (1977) equation 4 for the CMAS runs. While Lindsley et al.'s pyroxene thermometers are based on the most complex solution model, Wells's equation is based on the simplest ideal-solution model; hence, the above comparison brings out the relative practical usefulness of these variably complicated thermometers. From Table 5 it is clear that Lindsley et al.'s thermometers cannot reproduce the CMAS data at all, whereas the

simple ideal solution-based thermometer of Wells correctly reproduces the experimental CMAS data. Such a strange result was not expected and is not fully understood. It seems possible that the "excess" parameters (which are, in reality, curve-fitting parameters), derived by Lindsley et al. from the CMS data, add cumulative errors to the estimated temperatures for the CMAS runs.

In order to facilitate comparison of the CMAS data with the well-reversed 20 kbar data of Danckwerth and Newton on the system MAS, Al₂O₃ in enstatite is approximated by the reaction (B) above. For this reaction,

$$K_B = \frac{a_{\text{Fo}}^{\text{ol}} \cdot a_{\text{MgTs}}^{\text{opx}}}{a_{\text{MgAl}_2\text{O}_4} \cdot a_{\text{En}}^{\text{cpx}}} \quad (1)$$

Since in the CMAS system spinel and forsterite are nearly pure phases, $a_{\text{Fo}}^{\text{ol}} \approx a_{\text{MgAl}_2\text{O}_4}^{\text{sp}} \approx 1.0$. Assuming an ideal solution model for Al, Mg exchange, K_B can be simply related to mole fractions, following a Wood and Banno (1973) approach:

$$K_B = \left(\frac{X_{\text{Al}}^{\text{Ml}}}{X_{\text{Mg}}^{\text{Ml}}}_{\text{opx}} \right) \quad (2)$$

Figure 9 shows a $\ln K_B$ vs. $1/T$ type plot of the CMAS data obtained in the present study; experimental data on CMAS and MAS systems by some previous workers are also compared. An optimum linear fit (fitted by eye) to the best set of reversed data obtained in the present study gives the equation

$$T_B(\text{K}) = 3666 / (0.8808 - \ln K_B) \quad (3)$$

As pointed out earlier, Al in enstatite in the spinel periodotite field seems to be virtually independent of P in the MAS and CMAS systems. Therefore $\int_1^P \Delta \bar{V} dP$ for reaction (B) must be very small (i.e., $\Delta \bar{V} \rightarrow 0$) and can be neglected. ΔH° and ΔS° calculated for reaction (B) from the relation

$$\ln K_B = -\frac{\Delta H^\circ}{RT} + \frac{\Delta S^\circ}{R} \quad (4)$$

are 7.284 kcal mol⁻¹ and 1.75 cal mol⁻¹K⁻¹, respectively.

Table 5. Comparison of thermometric estimates

P(kb)	T(°C)	$x_{\text{En}}^{\text{opx}}$	$x_{\text{En}}^{\text{cpx}}$	$x_{\text{Di}}^{\text{opx}}$	$x_{\text{Di}}^{\text{cpx}}$	T(in °C)			
						Wells	T _B (text)	T _{A1} (LGD.81)	T _{A2} (LGD.81)
12.5	900	.871	.051	.024	.835	909	897	622	817
14.5	900	.875	.095	.029	.804	1047	922	799	894
10	900	.881	.068	.021	.836	968	915	706	791
10	1000	.838	.069	.037	.786	983	1015	669	901
12.5	1000	.831	.077	.036	.803	1007	1007	718	886
12.5	1150	.798	.124	.049	.713	1134	1192	761	970
15	1200	.789	.118	.043	.70	1127	1166	724	934
15	1000	.840	.082	.031	.79	1016	1016	725	872

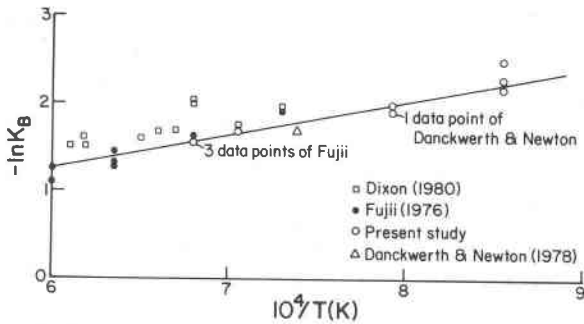


Fig. 9. $-\ln K_B$ vs temperature (in K) relationship of the data of present study are compared with those of Fujii (1976), Danckwerth and Newton (1978), and Dixon (1980). $K_B = (X_{\text{Al}}^{\text{Ml}}/X_{\text{Mg}}^{\text{Ml}})_{\text{opx}}$. The line is eye-fitted to the best set of data obtained in the present study.

The ΔH° value estimated is within uncertainty of the calorimetrically measured value of $\Delta H^\circ = 8.53 \pm 1.92$ kcal mol^{-1} of Charlu et al. (1975). This correspondence is excellent, considering all the simplistic assumptions made above.

Figure 9 and Table 5 show that the presently obtained CMAS data correspond well with the MAS data of Danckwerth and Newton (1979) and Fujii (1976). However, the CMAS data points of Dixon (1980) in the spinel peridotite field all lie above the best-fit line.

Table 5 shows that the uncertainty in the estimated temperature from equation (3) is high ($\pm 70^\circ\text{C}$). Uncertainties arise from (1) microprobe analysis ($\pm 5\%$ of the absolute value of Al_2O_3) (2) the width of the overlap region from which the equilibrium composition was inferred, and (3) $P(\pm 0.25$ kbar) and $T(\pm 4^\circ\text{C})$ measurements. Also, these errors propagate in a manner shown by Powell (1978). At lower temperatures the uncertainties are higher than at higher temperatures. At about 900°C and 12.5 kbar a cumulative uncertainty in the measured value of $(\text{Al}_2\text{O}_3)_{\text{opx}}$ is about 16%, whereas it is about 7% at 1200°C and at same pressure.

Ganguly and Ghose (1979) argued that Al_2O_3 in enstatite can be approximated as an ideal solution if treated as $\text{Mg}_3\text{Al}_2\text{Si}_3\text{O}_{12}$ component. In the present study, such a treatment was also carried out (not shown here) however, no significant improvement in T -estimates for the CMAS runs was achieved. Also, the close correspondence of ΔH° values using the ideal-solution model with the calorimetrically measured value suggests that the treatment of the aluminous opx "end-member" as $\text{Mg}_3\text{Al}_2\text{Si}_3\text{O}_{12}$ may be unnecessary (see also Danckwerth and Newton, 1979).

In conclusion, it appears that Wells' (1977) thermometer, in spite of its simplicity and somewhat erroneous assumptions (i.e., ideality of pyroxene solid solutions), can reproduce both CMS and CMAS data within experimental and analytical uncertainty. Rigorous solution models, such as those of Lindsley et al. (1981), do not reproduce the CMAS data well. The thermometer presented above, based on the Al_2O_3 in opx_{ss}, has relatively high uncertainty. Considering these facts, Wells' (1977) thermometer appears to be most

suitable for the estimation of temperature of equilibration of natural spinel peridotites.

Acknowledgments

During initial stages of this work, much assistance was provided (including supply of furnace parts) by D. C. Presnall, A. L. Boettcher, S. R. Bohlen, and R. Luth. Discussions with them and W. G. Ernst, W. D. Carlson, J. Ganguly, G. Bussod and C. Ross have been helpful. The manuscript was reviewed by W. G. Ernst, D. C. Presnall, A. L. Boettcher, J. Munoz and W. A. Dollase. Official reviews by D. H. Lindsley and D. Perkins III have resulted in substantial improvement of the manuscript. R. E. Jones helped me with the probe work, including taking BSE and X-ray scanning pictures. P. Koch and M. W. Wegner taught me the etching technique used here. J. M. Christie and A. L. Boettcher kindly allowed the use of their microscopes for taking photomicrographs. I am indebted to R. Alkaly for taking extreme care in making the doubly polished thin sections. I am equally grateful to C. McCann and J. Guenther for their help with typing and drafting of this manuscript. Financial support from NSF grant EAR 82-11625 (to W. G. Ernst) is gratefully acknowledged.

References

- Akella, J. (1976) Garnet pyroxene equilibria in the system $\text{CaSiO}_3\text{-MgSiO}_3\text{-Al}_2\text{O}_3$ and in a natural mineral mixture. *American Mineralogist*, 61, 589-598.
- Bonatti, E. and Hamlyn, P. R. (1980) Oceanic ultramafic rocks. In C. Emiliani, Ed., *The Oceanic Lithosphere*, p. 241-283. J. Wiley & Sons, New York.
- Charlu, T. V., Newton, R. C., and Kleppa, O. J. (1975) Enthalpies of formation at 970 K of compounds in the system $\text{MgO-Al}_2\text{O}_3\text{-SiO}_2$ from high temperature solution calorimetry. *Geochimica et Cosmochimica Acta*, 39, 1487-1497.
- Danckwerth, P. A. and Newton, R. C. (1978) Experimental determination of the spinel peridotite to garnet peridotite reaction in the system $\text{MgO-Al}_2\text{O}_3\text{-SiO}_2$ in the range $900^\circ\text{-}1100^\circ\text{C}$ and Al_2O_3 isopleths of enstatite in the spinel field. *Contributions to Mineralogy and Petrology*, 66, 189-201.
- Dixon, J. R. (1980) A Spinel Lherzolite Barometer. Ph.D. Dissertation, University of Texas at Dallas.
- Fujii, T. (1976) Solubility of Al_2O_3 in enstatite coexisting with forsterite and spinel. *Carnegie Institution of Washington Yearbook*, 75, 566-571.
- Ganguly, J. and Ghose, S. (1979) Order-disorder in aluminous orthopyroxene and its petrologic implications. *Contributions to Mineralogy and Petrology*, 69, 375-385.
- Grover, J. E. (1980) Thermodynamics of pyroxenes. In C. T. Prewitt, Ed., *Pyroxenes*, 7, *Reviews in Mineralogy*, p. 213-288. Mineralogical Society of America, Washington, D. C.
- Hamilton, D. L. and Henderson, C. M. B. (1968) The preparation of silicates compositions by a gelling method. *Mineralogical Magazine*, 36, 832-838.
- Herzberg, C. T. and Chapman, N. A. (1976) Clinopyroxene geothermometry of spinel lherzolites. *American Mineralogist*, 61, 626-637.
- Howells, S. and O'Hara, M. J. (1975) Palaeogeotherms and the diopside-enstatite solvus. *Nature*, 254, 406-408.
- Johannes, W., Bell, P. M., Mao, H. K., Boettcher, A. L., Chipman, D. W., Hays, J. F., Newton, R. C., and Seifert, F. (1971) An interlaboratory comparison of piston-cylinder pressure calibration using the albite breakdown reaction. *Contributions to Mineralogy and Petrology*, 32, 24-38.
- Lane, D. L. and Ganguly, J. (1980) Al_2O_3 solubility in ortho-

- pyroxene in the system $\text{MgO-Al}_2\text{O}_3\text{-SiO}_2$: A re-evaluation and Mantle geotherm. *Journal of Geophysical Research*, 85, 6963-6972.
- Lindsley, D. H. and Dixon, S. A. (1976) Diopside-enstatite equilibria at 850°-1400°C and 5-35 kbar. *American Journal of Science*, 276, 1285-1301.
- Lindsley, D. H., Grover, J. E. and Davidson, P. M. (1981) The thermodynamics of the $\text{Mg}_2\text{Si}_2\text{O}_6\text{-CaMgSi}_2\text{O}_6$ join: a review and an improved model. In R. C. Newton, A. Navrotsky and B. J. Wood, Eds., *Advances in Geochemistry*, 1, p. 149-175. Springer, New York.
- Lofgren, G. E. (1980) Experimental studies on the dynamic crystallization of silicate melts. In R. B. Hargraves, Ed., *Physics of Magmatic Processes*, p. 487-551. Princeton University Press, Princeton.
- MacGregor, I. D. (1974) The system $\text{MgO-Al}_2\text{O}_3\text{-SiO}_2$: Solubility of Al_2O_3 in enstatite for spinel and garnet peridotite compositions. *American Mineralogist*, 59, 110-119.
- MacGregor, I. D. and Basu, A. R. (1974) Thermal structure of the lithosphere: A petrologic model. *Science*, 185, 1007-1011.
- Mori, T. (1977) Geothermometry of Spinel lherzolites. *Contributions to Mineralogy and Petrology*, 59, 261-279.
- Mori, T. and Green, D. H. (1975) Pyroxenes in the system $\text{Mg}_2\text{Si}_2\text{O}_6\text{-CaMgSi}_2\text{O}_6$ at high pressure. *Earth and Planetary Science Letters*, 26, 277-286.
- Obata, M. (1976) The solubility of Al_2O_3 in orthopyroxene in spinel and plagioclase peridotites and spinel pyroxenite. *American Mineralogist*, 61, 804-816.
- Perkins, D. and Newton, R. C. (1980) The compositions of coexisting pyroxenes and garnet in the system $\text{CaO-MgO-Al}_2\text{O}_3\text{-SiO}_2$ at 900°-1100°C and high pressures. *Contributions to Mineralogy and Petrology*, 75, 291-300.
- Powell, R. (1978) The thermodynamics of pyroxene geotherms. *Philosophical Transactions, Royal Society of London*, A288, 475-469.
- Presnall, D. C. (1976) Alumina content of enstatite as a geobarometer for plagioclase and spinel lherzolites. *American Mineralogist*, 61, 582-583.
- Ringwood, A. E. (1975) *Composition and Petrology of the Earth's Mantle*. McGraw-Hill, New York.
- Sen, G. (1983) A petrologic model for the constitution of the upper mantle and crust of the Koolau shield, Oahu, Hawaii, and Hawaiian magmatism. *Earth and Planetary Science Letters*, 62, 215-228.
- Warner, R. D. and Luth, W. C. (1974) The diopside-orthoenstatite two-phase region in the system $\text{CaMgSi}_2\text{O}_6\text{-Mg}_2\text{Si}_2\text{O}_6$. *American Mineralogist*, 59, 98-109.
- Wegner, M. W., Jones, R. E., and Christie, J. M. (1978) Exsolution in terrestrial and lunar plagioclases revealed by chemical etching. *Contributions to Mineralogy and Petrology*, 65, 283-291.
- Wells, P. R. A. (1977) Pyroxene phase equilibria at low pressure. In C. T. Prewitt, Ed., *Pyroxenes*, vol. 1, *Reviews in Mineralogy*, p. 213-288. Mineralogical Society of America, Washington, D. C.
- Wilshire, H. G., and Jackson, E. D. (1975) Problems in determining mantle geotherms from pyroxene compositions of ultramafic rocks. *Journal of Geology*, 83, 313-329.
- Wood, B. J. and Banno, S. (1973) Garnet-orthopyroxene and orthopyroxene-clinopyroxene relationships in simple and complex systems. *Contributions to Mineralogy and Petrology*, 42, 109-124.

*Manuscript received, July 7, 1983;
accepted for publication, March 14, 1985.*

Appendix I. Abbreviations used in the text.

Abbreviations used in the text:

opx	-- orthopyroxene
cpx	-- clinopyroxene
en	-- enstatite ($\text{Mg}_2\text{Si}_2\text{O}_6$)
di	-- diopside ($\text{CaMgSi}_2\text{O}_6$)
a_i^j	-- activity of component i in phase j .
H°	-- standard state enthalpy change of a reaction at a reaction at 1 bar, T_i .
S°	-- standard state entropy change of a reaction
\bar{V}	-- change in molal volume in a reaction
K_B	-- equilibrium constant (=distribution coefficient assumed in present study) of reaction B.
T_B	-- temperature estimated from equation 1.
C_p°	-- change in heat capacity
R	-- universal gas constant
CaTs	-- $\text{CaAl}_2\text{SiO}_6$
MgTs	-- $\text{MgAl}_2\text{SiO}_6$
opx_{ss}	-- orthopyroxene solid solution
cpx_{ss}	-- clinopyroxene solid solution

Appendix II. Representative analyses of clinopyroxenes.

Representative analyses of clinopyroxenes (d = dissolution, e = exsolution run)

Run #	SiO ₂	CaO	MgO	Al ₂ O ₃	Si	Ca	Mg	Al	T(°C)	P(kb)
CMAS-H1-4	51.00	22.34	18.05	8.55	1.822	0.855	0.961	0.360		
CMAS-1X-3	51.71	23.50	18.17	6.13	1.863	0.907	0.976	0.260		
	51.28	22.86	18.38	7.03	1.844	0.881	0.985	0.298		
e	52.76	23.25	18.81	4.87	1.895	0.895	1.007	0.206		
	51.64	23.26	18.19	7.52	1.838	0.887	0.965	0.315		
	52.22	23.10	18.72	6.47	1.859	0.881	0.993	0.272	900	14.5
CMAS-H2-4	55.39	23.62	20.82	1.01	1.968	0.899	1.102	0.042		
	54.39	24.20	19.14	3.57	1.925	0.918	1.010	0.149		
d	54.98	24.17	19.54	2.46	1.948	0.918	1.032	0.103		
	54.67	23.42	20.09	2.77	1.938	0.890	1.061	0.116		
	54.24	24.72	18.71	1.73	1.962	0.958	1.008	0.074		
CMAS-2X-3	52.19	24.02	17.90	6.05	1.870	0.922	0.956	0.255		
	52.44	23.70	17.90	5.52	1.887	0.914	0.960	0.234		
d	52.33	24.46	16.65	5.45	1.874	0.939	0.942	0.247		
	53.45	23.76	17.86	4.79	1.915	0.912	0.954	0.202		
CMAS-2Y-3	52.30	22.34	18.95	6.65	1.862	0.852	1.005	0.279	900	12.5
e(Recycled)	52.80	23.56	17.53	6.46	1.881	0.899	0.931	0.271		
	53.69	23.31	18.27	4.90	1.905	0.901	0.957	0.204		
CMAS-1X-2	54.26	23.53	18.11	4.85	1.923	0.894	0.956	0.203		
d	53.59	24.33	18.41	4.48	1.903	0.924	0.977	0.188		
	54.81	24.27	18.85	5.36	1.886	0.911	0.985	0.322	900	10
CMAS-2Y-2	Very similar to the above range									
e	Very similar to the above range									
Run #	SiO ₂	CaO	MgO	Al ₂ O ₃	Si	Ca	Mg	Al	T(°C)	P(kb)
CMAS-1X-R1	51.55	23.21	18.70	6.52	1.848	0.891	0.999	0.276		
e	51.25	23.11	18.14	6.37	1.857	0.897	0.980	0.272	1000	12.5
	50.86	21.97	19.33	7.66	1.821	0.843	1.032	0.323		
CMAS-1	51.34	23.13	17.46	7.99	1.835	0.886	0.930	0.337		
	53.50	22.81	18.59	6.09	1.888	0.862	0.977	0.253		
e*	51.13	22.36	17.85	7.35	1.846	0.865	0.960	0.313	1000	10
CMAS-1X-R2	52.20	22.58	18.55	6.51	1.867	0.865	0.989	0.274		
d	52.71	24.02	19.24	5.64	1.863	0.909	1.013	0.235		
	51.84	23.42	18.92	5.18	1.872	0.906	1.019	0.220		
CMAS-5	52.34	22.96	18.91	7.75	1.835	0.862	0.988	0.320		
e*	51.86	23.40	18.02	6.76	1.857	0.898	0.959	0.285	1000	9.5
	51.85	23.13	18.63	7.03	1.844	0.882	0.988	0.295		
CMAS-3	50.99	23.72	17.80	6.33	1.853	0.924	0.964	0.271		
e*	49.85	22.99	17.57	7.92	1.818	0.898	0.955	0.341	1000	9
	51.60	22.97	18.30	8.93	1.812	0.684	0.957	0.369		
	52.73	23.02	19.58	6.41	1.854	0.867	1.026	0.266		
CMAS-1X-2	52.73	22.79	18.94	7.85	1.840	0.852	0.985	0.323		
d (q)	53.81	20.05	21.88	6.85	1.857	0.742	1.125	0.279	1150	12.5
CMAS-2Y-2	49.78	22.16	17.65	9.09	1.802	0.860	0.953	0.388		
e	51.13	22.11	18.38	8.66	1.807	0.865	0.968	0.361		

SEN: PYROXENE COMPOSITIONS IN SYSTEM $\text{CaO-MgO-Al}_2\text{O}_3\text{-SiO}_2$

APPENDIX-II (Con't)										
Run #	SiO ₂	CaO	MgO	Al ₂ O ₃	Si	Ca	Mg	Al	T(°C)	P(kb)
	52.71	22.59	18.80	7.80	1.840	0.848	0.978	0.320		
CMAS-2Y-1	50.25	22.95	18.27	9.67	1.780	0.871	0.964	0.404		
e	49.76	22.16	17.65	9.09	1.802	0.860	0.953	0.380		
	49.79	22.46	18.34	9.56	1.779	0.860	0.477	0.403	1200	15
	52.84	22.94	19.04	8.08	1.834	0.853	0.984	0.330		
CMAS-1X-1	52.01	22.78	18.41	8.72	1.822	8.55	0.961	0.360		
d	52.57	22.80	19.29	6.45	1.859	0.864	1.016	0.269	1200	15
CMAS-6	50.68	20.54	21.34	7.45	1.816	0.785	1.134	0.303		
e*	51.09	23.27	19.77	6.15	1.844	0.883	1.043	0.256	900	9
CMAS-H2-5	53.05	17.10	23.63	6.39	1.862	0.643	1.236	0.265		
	52.72	24.23	18.22	5.59	1.878	0.925	0.956	0.236		
d	55.25	22.95	20.72	2.82	1.939	0.863	1.084	0.116		
CMAS-H1-5	52.11	23.99	16.95	7.29	1.844	0.910	0.946	0.304		
e	53.35	24.64	18.48	3.08	1.927	0.954	0.995	0.131		
	52.24	24.30	18.31	5.21	1.877	0.935	0.980	0.221	1000	15
	53.25	23.68	18.56	6.80	1.862	0.887	0.968	0.280		
	52.56	23.94	18.43	5.40	1.880	0.917	0.982	0.228		
CMAS-1X-2	52.02	23.93	17.72	5.96	1.873	0.924	0.951	0.253		
	52.94	22.47	17.92	5.74	1.877	0.887	0.984	0.249		
d	51.49	23.87	17.38	7.04	1.851	0.919	0.931	0.298		
	52.03	23.91	18.47	4.89	1.891	0.903	1.000	0.209		
	52.21	23.41	17.08	6.69	1.851	0.925	0.938	0.291		
	51.19	22.50	18.15	6.24	1.866	0.879	0.986	0.268		
	52.06	23.34	18.00	5.62	1.883	0.904	0.970	0.239		
CMAS-H2-2	52.89	22.33	19.62	5.86	1.874	0.848	1.036	0.245		
	52.24	23.59	17.83	5.34	1.891	0.915	0.962	0.228		
	53.34	24.14	18.33	5.15	1.894	0.918	0.970	0.215	1000	12.5
d	52.63	23.73	18.62	5.38	1.880	0.908	0.992	0.226		
	62.06	23.67	18.07	5.79	1.874	0.913	0.970	0.246		
e*	These are run products from gel starting material. The composition range exhibited by each of this run, in comparison to its corresponding dissolution run, suggests that they are mostly 'exsolution' (see also discussion of Warner and Luth, 1974; Lindsley and Dixon, 1976). However, it is possible that a few nuclei of crystals (as shown by x-ray diffraction) were present, and therefore, some crystals may actually exhibit 'dissolution' reaction									
q	Quench crystals.									

Appendix III. Representative analyses of orthopyroxenes.

Representative analyses of orthopyroxenes

Run #	SiO ₂	CaO	MgO	Al ₂ O ₃	Si	Ca	Mg	Al	T(°C)	P(kb)
	55.85	0.89	36.94	8.42	1.835	0.031	1.809	0.326		
CMAS-H1-4	55.55	1.15	36.95	4.85	1.894	0.042	1.878	0.195		
CMAS-1X-3	55.52	0.92	36.79	8.73	1.827	0.032	1.805	0.339		
e	55.72	1.25	37.26	6.72	1.855	0.045	1.849	0.264		
	56.47	1.31	37.38	7.30	1.352	0.046	1.827	0.282		
	54.27	0.99	36.08	8.18	1.331	0.030	1.814	0.326	900	14.5
	58.31	1.06	38.38	3.46	1.932	0.038	1.895	0.135		
CMAS-H2-4	56.85	0.93	37.82	5.06	1.895	0.033	1.879	0.199		
	56.78	0.97	37.68	4.40	1.908	0.035	1.687	0.174		
d	57.92	1.07	38.47	3.57	1.924	0.038	1.904	0.140		
CMAS-2X-3	56.97	0.74	37.67	5.86	1.886	0.026	1.859	0.229		
	57.57	0.89	37.85	5.04	1.904	0.031	1.866	0.197		
d	56.48	1.04	37.14	5.26	1.896	0.037	1.858	0.208		
	57.10	0.82	37.48	5.31	1.900	0.029	1.859	0.208		
	57.15	0.76	37.71	6.04	1.884	0.027	1.853	0.235		
(q)	53.30	0.30	36.03	9.94	1.796	0.011	1.806	0.394	900	12.5
CMAS-2Y-3(q)	53.89	0.56	35.81	10.14	1.800	0.020	1.782	0.399		
e	56.79	0.73	37.69	6.73	1.868	0.026	1.847	0.261		
	56.12	0.72	36.72	4.92	1.908	0.026	1.861	0.145		
(q)	55.18	0.59	36.44	9.13	1.825	0.021	1.796	0.356		
	56.58	0.80	37.49	4.34	1.912	0.029	1.888	0.165		
Run #	SiO ₂	CaO	MgO	Al ₂ O ₃	Si	Ca	Mg	Al	T(°C)	P(kb)
CMAS-2X-2	57.44	0.77	37.93	3.31	1.937	0.028	1.902	0.131		
	56.54	0.57	37.86	5.10	1.894	0.021	1.890	0.202		
	57.08	0.57	37.97	5.59	1.890	0.020	1.873	0.218		
	56.70	0.61	38.35	4.56	1.898	0.022	1.913	0.180		
CMAS-2Y-2	56.48	0.51	37.06	7.31	1.865	0.018	1.824	0.185	900	10
e	56.77	0.64	37.60	4.94	1.903	0.023	1.878	0.195		
	55.19	0.72	36.36	7.27	1.858	0.026	1.824	0.289		
CMAS-H2-5	54.79	0.85	35.88	7.50	1.855	0.031	1.810	0.300		
d	56.12	0.98	37.13	4.54	1.906	0.036	1.880	0.182		
	54.88	1.22	36.31	5.31	1.886	0.045	1.860	0.215	1000	15
CMAS-H1-5	55.95	0.86	37.17	7.14	1.856	0.030	1.838	0.279		
e (q)	53.39	1.15	35.45	10.47	1.786	0.041	1.767	0.413		
	56.10	1.09	37.48	5.64	1.878	0.039	1.870	0.223		
	58.00	1.98	37.45	0.78	1.985	0.073	1.910	0.031		
CMAS-1X-2	54.28	1.40	35.03	6.50	1.874	0.052	1.803	0.265		
d	54.72	0.78	36.12	7.77	1.846	0.028	1.816	0.309		
	56.29	1.16	36.93	6.79	1.868	0.038	1.827	0.266		
CMAS-H2-2	55.61	1.84	36.27	6.56	1.866	0.066	1.813	0.259		
d	56.09	0.80	36.94	7.30	1.859	0.038	1.825	0.285		
	54.86	1.13	36.10	7.88	1.842	0.041	1.807	0.312	1000	12.5

SEN: PYROXENE COMPOSITIONS IN SYSTEM $CaO-MgO-Al_2O_3-SiO_2$

CMAS-1X-R1	53.71	1.10	36.56	8.27	1.814	0.040	1.839	0.329		
	54.43	1.04	36.61	8.49	1.819	0.037	1.823	0.335		
	55.79	0.79	37.19	5.01	1.895	0.027	1.882	0.260		
Run #	SiO ₂	CaO	MgO	Al ₂ O ₃	Si	Ca	Mg	Al	T(°C)	P(kb)
CMAS-1	54.83	1.42	36.07	7.67	1.842	0.051	1.806	0.304		
e*	55.01	0.68	37.16	8.01	1.831	0.024	1.843	0.314	1000	10
CMAS-1X-R2	56.17	1.03	38.24	6.76	1.855	0.036	1.863	0.260		
	56.79	0.95	38.56	5.77	1.870	0.033	1.891	0.242		
	55.75	0.90	37.66	6.37	1.860	0.032	1.872	0.250		
d	55.69	0.86	37.53	6.15	1.866	0.031	1.874	0.243		
	55.72	0.89	37.60	6.03	1.867	0.032	1.677	0.238		
CMAS-5	54.70	1.05	36.64	6.85	1.852	0.038	1.849	0.273		
e*	56.18	1.30	37.14	5.88	1.878	0.047	1.850	0.232	1000	9.5
	55.10	1.16	36.22	6.33	1.872	0.042	1.834	0.254		
	7.74	1.17	38.21	4.09	1.915	0.041	1.888	0.160		
CMAS-3	55.47	1.51	36.59	5.40	1.884	0.055	1.852	0.216	1000	9
e*	54.75	0.98	37.30	5.83	1.862	0.036	1.890	0.234		
(q)	53.67	0.81	36.41	8.67	1.811	0.029	1.831	0.345		
CMAS-1X-2'	54.86	1.60	35.67	7.73	1.847	0.058	1.789	0.307		
d	55.15	1.54	36.73	7.05	1.847	0.055	1.833	0.278		
	55.08	1.27	36.18	6.76	1.863	0.046	1.823	0.270		
	55.05	1.17	36.29	7.50	1.848	0.042	1.816	0.297	1150	12.5
CMAS-2Y-2'	54.59	1.39	36.55	8.05	1.825	0.050	1.824	0.318		
	54.77	1.24	36.40	8.08	1.832	0.044	1.815	0.319		
e	54.59	1.24	35.95	8.27	1.833	0.044	1.799	0.328		
Run #	SiO ₂	CaO	MgO	Al ₂ O ₃	Si	Ca	Mg	Al	T(°C)	P(kb)
CMAS-1X-1	56.12	1.24	36.98	5.20	1.893	0.045	1.859	0.208		
	55.22	1.48	36.17	8.74	1.826	0.052	1.783	0.341		
d	54.11	1.61	36.64	8.57	1.807	0.057	1.823	0.337		
	54.43	1.17	36.36	8.51	1.821	0.042	1.813	0.336	1200	15
CMAS-2Y-1	53.71	1.52	34.87	9.89	1.805	0.055	1.747	0.392		
e	55.88	1.10	36.84	9.12	1.822	0.039	1.791	0.351		
	54.21	1.59	36.43	8.04	1.821	0.057	1.824	0.318		

Appendix IV. Analyses of pyroxenes in two "tie-line rotation" experiments.

	Run # (AEDS-1, AEDS-1) # 1		# 2	
	12.5 kb/950°C		12.5 kb/1050°C	
	cpx	opx	cpx	opx*
SiO ₂	53.97(±.50)	58.16(.40)	52.07(.5)	55.97(.5)
CaO	23.46(.46)	0.92(.20)	23.03(.7)	1.09(.4)
MgO	19.06(.3)	38.10(.5)	18.88(.6)	37.81(.8)
Al ₂ O ₃	5.35(.4)	4.93(.8)	6.84(.3)	7.25(1.1)
Si	1.894	1.909	1.848	1.842
Ca	0.883	0.032	0.876	0.039
Mg	0.997	1.863	0.999	1.855
Al	0.221	0.191	0.286	0.281

*Grains too small, not too many good analyses

The above are two runs using (c) and (d) reversal combination (see the section on experimental approach). Compositions of the starting Aluminous OPx_{ss} and CPx_{ss} are the same as in table 1 of the text.